Beneficial effects of combination therapy of canagliflozin and teneligliptin on diabetic polyneuropathy and β-cell volume density in spontaneously type 2 diabetic Goto-Kakizaki rats.

(自然発症 2 型糖尿病モデル Goto-Kakizaki ラットにおける糖尿病性神経障害と β 細胞容積に対するカナグリフロジンとテネリグリプチンの併用療法の効果について)

申 請 者　弘前大学大学院医学研究科
病態制御科学領域病態病理学教育研究分野
郭　丹陽

指導教授　　水上浩哉

Abstract

Aims: Parasympathetic nerve (PN) signaling plays a crucial role in the maintenance of pancreatic β-cell volume density (V_β). PN may be pathologically affected in diabetic polyneuropathy (DPN). However, the association between the reduction of PNs in islets and V_β and the therapeutic effects of a DPP4 inhibitor (DPP4i) and an SGLT2 inhibitor (SGLT2i) in nonobese type 2 diabetes mellitus (T2DM) Goto-Kakizaki rats (GK) have not been investigated.

Materials and Methods: We divided 5-week old male GK and Wistar rats (W) into a DPP4i-treated group (GKTe), SGLT2i-treated group (GKCa), and combination-treated group (GKCaTe). After 25 weeks, the pancreata was pathologically evaluated.

Results: V_β in GK was significantly decreased ($p < 0.01$ vs. W), whereas V_β was the most well preserved in GKCaTe ($p < 0.05$ vs. GKTe), followed by GKTe ($p < 0.05$ vs. GK). The decreased amount of PNs in the islets and intraepidermal nerve fiber density (IENFD) in GK was significantly improved in the treated groups compared with GK ($p < 0.05$ vs. GKCa and GKTe and $p < 0.01$ vs. GKCaTe). PN density and IENFD were significantly correlated with V_β ($r = 0.55$, $p < 0.01$ and $r = 0.54$, $p < 0.01$, respectively). IENFD was identified as a surrogate marker for the prediction of V_β (cutoff value, 16.39).

Conclusions: The combination therapy of DPP4i and SGLT2i improved V_β accompanied by PNs density and IENFD. IENFD was proportionally correlated with V_β. Therefore, the prevention of DPN development may be concurrently beneficial for the preservation of V_β in nonobese T2DM.

Abbreviations

T2DM; Type 2 diabetes mellitus, DPN; Diabetic polyneuropathy, GK rats; Goto-Kakizaki (GK) rats, DPP4i; Dipeptidyl peptidase 4 inhibitor, SGLT2i; Sodium glucose cotransporter inhibitor, OGTT; Oral glucose tolerance test, GLP-1; Glucagon-like peptide-1, PN; Parasympathetic nerve, VAChT; Vesicular acetylcholine transporter, MNCV; Motor nerve conduction velocity, SNCV;

Sensory nerve conduction velocity, IENFD; Intraepidermal nerve fiber density, ROC; Receiver operating characteristic, AUC; Area under the curve

1. Introduction

Pathological changes of the pancreas in type 2 diabetes mellitus (T2DM) are mainly characterized by reduced pancreatic β-cell volume density (V_β) [1-4]. Currently, V_β regeneration is one of the promising therapeutic targets for T2DM. The underlying mechanisms of those changes are assumed to be an increase in oxidative stress, endoplasmic reticulum stress, and a deficit of autophagy induced by abnormal glucose metabolism and amyloid deposition in T2DM [4-7].

The pancreas is richly innervated by autonomic fibers [8-12]. Neuronal signals, especially those transmitted via the vagal nerves, are known regulators of both the functioning and the proliferation of β-cells [13-16]. The neuronal input from the liver to the pancreas via a branch of the vagus nerve stimulates the secretion of neurotransmitters from the nerve ends, leading to β-cell proliferation [17, 18]. These findings suggest that functional vagal innervation equipped with a sufficient number of nerve endings is indispensable in β-cell proliferation.

Diabetic polyneuropathy (DPN) develops from initial small unmyelinated nerve fiber loss into late structural changes of large myelinated nerve fiber loss during its natural course [19]. In addition to sensory neuropathy, the amount of small fibers of autonomic nerves may decrease. Autonomic innervation into the islets was significantly decreased in severely hyperglycemic T2DM Chinese hamsters accompanied with islet dysfunction and in human type 1 diabetes patients, while no apparent sympathetic nerve reduction was observed in the islets of Western T2DM autopsy cases [20, 21]. The autonomic innervation of the islets may be pathologically altered in nonobese T2DM, but this has not been thoroughly evaluated [21].

Here we evaluated the pathological changes of parasympathetic innervation to the islets and its correlation with V_β and DPN in Goto-Kakizaki (GK) rats, a nonobese T2DM model, which have clinical and pathological similarities with Japanese patients [22, 23]. We also explored the beneficial effects of combination therapy of a DPP4 inhibitor (DPP4i) and an SGLT2 inhibitor (SGLT2i) compared with monotherapy on V_β relating to the pathology of parasympathetic

innervation.

2. Material and methods

2.1. Animals

We purchased 5-week-old (approximately 1 week after weaning) male GK rats (GK) and Wistar rats (W) from CLEA Japan, Inc. (Tokyo, Japan). GK and W were sacrificed after the evaluation of neurological functions and glucose metabolism (n = 8) at 5 weeks of ages as a baseline control. They were housed in polycarbonate cages, each containing 3 rats, with wire lids and hardwood chips for bedding and with a 12-h light/dark cycle in SPF condition. They were divided into four groups（n=7-8）that were orally administered at 18:00 a daily dose of 10 mg/kg of an SGLT2i (canagliflozin, Ca), a DPP4i (teneligliptin, Te), or both (CaTe) (provided by Mitsubishi Tanabe Pharma Corporation, Osaka, Japan). This dose was expected to enhance insulin secretion and β-cell proliferation based on the results of previous studies [24, 25]. An untreated group (vehicle only) was used as the control. The treatment continued for 24 weeks, and the rats were 29 weeks old by then. The animals were fed a standard CE-2 rodent diet (CLEA Japan, Inc.) *ad libitum*.

The body weight and food intake of each rat were measured every two weeks. At the start of the study and at 24 weeks, we performed a 2 g/kg oral glucose tolerance test (OGTT) after an overnight fast and measured plasma insulin levels and active glucagon-like peptide-1 (GLP-1) before (i.e., fasting) and 15 min after the glucose challenge. At the end of the study, following an overnight fast, the rats were euthanized with an overdose of isoflurane. The pancreas and the skin of plantar in hind limb were resected in the animal facility of Hirosaki University School of Medicine. A total of 55 rats were used.

All of the procedures followed the Principles of Laboratory Animal Care (National Institutes of Health publication no. 85–23, revised 1985) and the institutional guidelines of

Hirosaki University Animal Experimentation for the care and use of laboratory animals (approval #M05032).

2.2. Measurement of blood glucose, insulin, GLP-1, glycated hemoglobin (HbA1c) and pancreatic insulin content

Blood glucose from tail tip was measured using a OneTouch Verio IQ test (Johnson and Johnson, Tokyo, Japan). Insulin levels were measured in plasma samples using enzyme-linked immunosorbent assay kits (Morinaga Institute of Biological Science, Yokohama, Japan). Active GLP-1 was measured at LSI Medicine Corporation (Tokyo, Japan). For sample preparation for active GLP-1 measurement, 300 µl of blood was collected from the tail vein after 16 h of fasting at 23–24 weeks of the experimental period. Ca, Te, or both compounds were orally administered 15 min before 2 g/kg total body weight glucose challenge. After 15 min of glucose stimulation, 300 µl of blood was collected for analysis. The blood samples were immediately mixed with 25 mg/ml ethylenediaminetetraacetic acid and 4 times diluted DPP-4 inhibitor (DPP-4-010; Merck KGaA, Darmstadt, Germany). The level of active GLP-1 was measured using an Active GLP-1 (ver. 2) Kit (Meso Scale Discovery, Gaithersburg, MD, USA), as per the manufacturer's protocol. The HbA1c level in whole blood was measured using a NycoCard READER II device (Axis-Shield PoC AS, Oslo, Norway). Pancreatic insulin content was measured as previously described [26]. Briefly, excised pancreatic tissues from the tail portion were homogenized using a ×10 acid-ethanol solution (0.2 N HCl/75 % ethanol) (vol/g) in a potter tube and then centrifuged at 15,000 rpm for 15 min at 4 °C. Then, the supernatant was used to measure the insulin level enzyme-linked immunosorbent assay (Morinaga Institute of Biological Science).

2.3. Histological evaluation of the islets

As a reference, the pancreas was obtained from 5 or 29-week-old GK and W and was fixed in 4% paraformaldehyde and embedded in paraffin. Then, tissue sections were stained with

hematoxylin and eosin (H&E) for review. All histological evaluations and morphometric analyses were performed by three investigators (DG, SO, and HM) who were blinded to the samples.

2.4. Morphometric analysis of islet endocrine cells

We performed immunohistochemistry on pancreas sections for the morphometric analysis. The antibodies used are listed in Table 1. The volume density of total endocrine cells was calculated using the point-counting method, as previously described, with slight modification [6,7,23,26,27]. First, a low magnification view (×10) of PGP9.5-stained sections of the whole pancreas was captured. The captured images were evaluated by ImageJ 1.47v software (NIH, Bethesda, MD, USA). The images were overlaid on a grid consisting of 625 points. The islet volume density was determined by dividing the total number of points on the islet cells by the total number of points on the pancreatic parenchyma and mesenchymal tissues. At least 120 images were evaluated for each pancreas.

To characterize the composition of islet endocrine cells, we conducted simultaneous immunostaining of four endocrine hormones (insulin, glucagon, somatostatin, and pancreatic polypeptide [PP]), and Ki67, as previously described [6,7]. Briefly, after deparaffinization and autoclave pretreatment for antigen retrieval, the sections were firstly incubated with an anti-Ki67 antibody, followed by a streptavidin-biotin-peroxidase system (Nichirei Co., Tokyo, Japan). Ki67 positive cells were colored as brown with a DAB Substrate Kit (Abcam PLC, Cambridge, United Kingdom). Secondly, they were incubated with an anti-PP antibody, followed by a streptavidin-biotin-alkaline phosphatase system (Nichirei Co.). PP positive cells were stained as blue with Ferangi Blue (Biocare Medical, Pacheco, CA, USA). Thirdly, the sections were incubated overnight with an anti-glucagon antibody, followed by incubation with a streptavidin-biotin-alkaline phosphatase system. Glucagon positive cells were colored as red with Vulcan Fast Red (Biocare Medical). Fourthly, the sections were incubated with an anti-insulin antibody, followed by a streptavidin-biotin-peroxidase system. Insulin positive cells were labeled as black with

Vector SG Substrate (Vector Laboratories Inc., Burlingame, CA, USA). Finally, the δ-cells were labeled with an anti-somatostatin antibody, reacted with a streptavidin-biotin-peroxidase system, and colored as green with a Vina Green chromogen kit (Biocare Medical). Thereafter, the sections were lightly counterstained with hematoxylin.

To determine the fractional β-, α-, δ- and PP-cell areas relative to the pancreatic parenchymal area (V_β, V_α, V_δ, and V_{PP}, respectively), the pancreatic sections were viewed at ×40 magnification (Axio-Imager A1, Carl Zeiss, Germany). V_β, V_α, V_δ, and V_{PP} were quantified on a point count basis using Image J [6,7,26]. A captured image of the five-color labeled sections was overlaid on a grid consisting of 1000 points. The population (%) of β-, α-, δ-, and PP-cells was determined by dividing the total number of points on each type of hormone-stained cells by the total number of points on the islet endocrine cells. The areas of blood vessels, nerves, fat, and connective tissues were excluded from these measurements. V_β, V_α, V_δ, and V_{PP} were calculated by multiplying V_i by the population of each type of endocrine cell obtained with morphometry for the five-color immunostained sections. At least 50 islets were examined in each case. The amount of proliferative cells that were double-positive for each islet hormone and Ki67 (among over 500 endocrine cells) was counted. For β-cell apoptosis, double immunostaining for insulin and terminal deoxynucleotidyl transferase dUTP nick end-labeling (Millipore, USA) was performed, as previously described [23,26,27].

2.5. Parasympathetic nerve (PN) fibers in islets

To explore the alteration of innervation into the islets by small PN fibers, we performed an immunohistochemical evaluation for vesicular acetylcholine transporter (VAChT), which was visualized as red dots in the islets. The number of VAChT nerve fibers was counted and divided by the islet area to obtain the density in each islet.

2.6. Nerve conduction velocities (NCVs)

NCVs were examined based on a previous study [28]. At 5 and 29 weeks of ages, motor nerve conduction velocity (MNCV) and sensory nerve conduction velocity (SNCV) were evaluated by electric stimulation (MEB-9102, Nihon Kohden Corp., Tokyo, Japan). An average of at least five recordings for each was used for measurements.

2.7. Tail-flick test

The tail-flick response to a thermal stimulus of radiant heat was measured using a heat stimulator (MK-330B, Muromachi Kikai Co., Ltd., Tokyo, Japan), as described previously [28]. At 5 and 29 weeks of age, the tail-flick latencies were measured ten times per session, separated by a minimum interval of 10 min. Tail movements as a result of voluntary locomotion were not measured.

2.8. Intraepidermal nerve fiber density (IENFD)

IENFD was evaluated using the skin of plantar in hind limb by double immunofluorescent staining, as previously described [28]. Briefly, epidermal nerve fibers were labeled with red fluorescence by anti-PGP9.5 antibody and the keratinocytes of the epidermis were labeled with green fluorescence by anti-CK 5/6 antibody. Nerve fibers in the epidermis were quantified and expressed as the number per mm distance of basal layer in the epidermis.

2.9. Statistics

Data are presented as mean ± standard error (SE). Statistical comparisons of the mean values among the groups were made by analysis of variance with Tukey's test using StatView 5.0.1 (SAS Institute Inc., Cary, NC, USA). A linear regression was performed for the correlation analysis. To identify the optimum IENFD cutoff points for the prediction of V_{β} reduction when low V_{β} was defined as < 1.28, receiver operating characteristic (ROC) curves and the area under

the curve (AUC) were calculated using JMP 10.0.4 software (SAS Institute Inc.). P-values < 0.05 were considered statistically significant.

3. Results

3.1. Laboratory findings and food intake (Table 2)

The body weight of GK at 5 weeks of age was comparable with W. The body weight gain of GK was less than that of W after 24 weeks ($p < 0.01$). In contrast to GKTe, Ca and combination treatment significantly decreased body weight ($p < 0.05$ vs. GK). Food intake was comparable between W, GK, and GKTe throughout the study. Ca and combination therapy significantly increased the food intake ($p < 0.05$ vs. GK). Te effectively decreased only fed glucose levels of GK ($p < 0.01$). In contrast, Ca and CaTe ameliorated both glucose levels of GK under fasting and fed conditions ($p < 0.05$ in fasting blood glucose and $p < 0.01$ in under fed blood glucose). Significant reductions in glycated hemoglobin were observed in all treatment groups ($p < 0.01$). Active GLP-1 in GK was comparable with that in W. In contrast to Ca, Te increased the level of active GLP-1 in GK by 11 times (fasting) and 4.6 times (glucose-stimulated) ($p < 0.05$ vs. GK). Notably, combination therapy further enhanced the level of active GLP-1 in both fasting and glucose stimulation conditions ($p < 0.01$ vs. GK, $p < 0.05$ vs. GKTe, and $p < 0.01$ vs. GKCa).

3.2. Glucose intolerance and insulin secretion (Figure 1)

Post-challenge hyperglycemia was already demonstrated in 5-week-old GK (**A**). At the end of the experiment, GK showed a more severe post-challenge hyperglycemia at 120 min than that of 5-week-old GK (**B**). Ca suppressed hyperglycemia more strongly than Te after the glucose challenge ($p < 0.05$). The combination treatment showed marked effect on the glucose intolerance of GK. Fasting plasma insulin concentrations were significantly suppressed in GKCa compared with GK ($p < 0.05$) (**C**). The insulin at 15 min after the glucose challenge was significantly

reduced in GK compared with W ($p < 0.01$). Te potentiated insulin secretion in GK ($p < 0.05$ vs. GK) and combination therapy evoked further insulin secretion ($p < 0.05$ vs. GKTe) (**C**). The Δ15 min insulin secretion level (insulin value at 15 min after the glucose challenge − insulin value at 0 min) showed 85 % reduction in GK compared with W ($p < 0.01$) (**D**). Ca showed a slight increase in Δ15 min insulin secretion, while Te potentiated Δ15 min insulin secretion ($p < 0.01$ vs. GK and $p < 0.05$ vs. GKCa). The GKCaTe had the highest Δ15 min insulin secretion among all groups ($p < 0.05$ vs. GKTe).

3.3. Islet morphometry (Table 3)

At 5 weeks of age, the islet contours of both W and GK were round and smooth in the H&E sections (**Figure 2, A**). In the sections labeled with five kinds of antibodies, the β-cells were located in the center of the islets and the α-, δ-, and PP-cells were located at the periphery (**Figure 2, B**). There was no significant difference in endocrine cell volume density between W and GK. At the end of the experiment, we observed irregular processes or budding of the endocrine cells admixing with interstitial stroma with the disturbance of the specific distribution of the endocrine cells in GK (**Figure 2, C and D**). V_β in GK was reduced by more than 50% compared with W ($p < 0.01$). GKCa showed the trend of amelioration of the islet contours and a slight increase in V_β **(Figure 2, C and D)**. Te increased V_β by 45% compared with GK ($p < 0.05$ vs. GK). Combination therapy exhibited the greatest effects on V_β among all groups ($p < 0.05$ vs. GKTe). V_α in GK was reduced by 37% compared with W ($p < 0.01$). Ca and Te had a minimal effect on V_α of GK, while combination therapy significantly increased V_α compared with GK ($p < 0.05$). This effect was also significant compared with Ca treatment ($p < 0.05$). V_δ was comparable among all groups. V_{PP} was dramatically (approximately 88%) reduced in GK compared with W ($p < 0.01$), but all treatments failed to restore the V_{PP} of GK.

3.4. Pancreatic insulin content (Table 3)

Supporting the morphometric data of the islets, the pancreatic insulin content of GK was decreased to 44% of that in W ($p < 0.01$). Ca slightly increased insulin content, while Te significantly recovered insulin content ($p < 0.05$ vs. GK), and combination therapy further ameliorated the insulin content ($p < 0.05$ vs. GKTe).

3.5. Proliferation and apoptosis of islet cells (Table 3)

At 5 weeks of age, Ki67-positive α-and β-cells were abundantly observed in the islets of both W and GK (**Figure 2)**. The frequency of Ki67 in β-cells in GK was reduced compared with W at 29 weeks of age. The frequency of Ki67-positive β-cells in GK treated with Ca exhibited a 70% reduction compared with that in W ($p < 0.01$) (**Figure 3)**. Te treatment increased β-cell proliferation by 2.3 times ($p < 0.05$ vs. GK), and combination therapy further ameliorated β-cell proliferation to similar level as W ($p < 0.01$ vs. GK). W showed a low proliferative activity of α- and δ-cells, while no proliferation of these cells was observed in GK. Mono- and combination therapies failed to recover δ-cell proliferation in GK. Ki67-positive PP-cells were not observed, except in W. The apoptotic cells in the islets were not observed in GK and W (data not shown).

3.6. PN innervation in islets (Figure 4)

At the beginning of the experiment, the density of VAChT in the islets was comparable between W and GK (**A, B and H**). However, at the end of the experiment, the density of VAChT was significantly decreased in GK compared with W ($p < 0.01$) (**C, D and I**). Ca treatment increased the density of VAChT ($p < 0.05$, **E and I**), and a further increase was observed in GKTe ($p < 0.01$, **F and I)**. The combination therapy exhibited the significant effects on VAChT density

in the islets ($p < 0.05$ vs. GK or GKTe, **G and I**). The density of VAChT was positively correlated with V_β ($p < 0.01$, $r = 0.55$, **J**).

3.7. Evaluation of peripheral nerve function and pathology

The MNCV and SNCV of GK were comparable to those of W at 5 weeks of age. Thermal latency was also similar (**Figure 5, A–C**). Immunofluorescence for intraepidermal small nerve fibers showed that IENFD was comparable between W and GK at 5 weeks of age (**Figure 5, D and E**). At the end of the experiment, no significant delays of MNCV and SNCV were observed in GK compared with those of W (**Figure 6, A**). Both monotherapy and combination therapy of Ca and Te had no impacts on NCVs of GK. On the contrary, in the tail-flick latency test, the thermal perception threshold in GK increased 2.5 times more than W at the end of experiment ($p < 0.01$) (**Figure 6, B**). This increase was significantly improved by Ca and Te treatment (both $p < 0.05$). Combination therapy significantly ameliorated the latency compared with each monotherapy ($p < 0.05$ vs. GKCa and GKTe). IENFD was reduced by 68% in GK compared with W ($p < 0.01$) (**Figure 6, C and D**). Monotherapy similarly improved these reductions (both $p < 0.05$ vs. GK). The greater effects were observed in the combination therapy group ($p < 0.01$ vs. GKCa and $p < 0.05$ vs. GKTe). IENFD proportionally correlated with V_β ($r = 0.54$, $p < 0.01$) (**Figure 6, E**). The ROC curve between V_β and IENFD showed the AUC as 0.87 when low V_β was defined as < 1.28 (**Figure 6, F**). The sensitivity and specificity of the test at a cutoff value of 16.39 were 0.86 and 0.82 respectively, indicating a good discrimination value.

4. Discussion

In the current study, GK showed a decrease in V_β, concomitant reduction of parasympathetic innervation to the islets, thermal threshold, and a reduction of IENFD correlating with V_β. Treatment with Ca significantly improved glycemic control, parasympathetic

innervation into the islets, and IENFD in GK. Nevertheless, the restoration of V_β and proliferation was insufficient compared with W. In contrast, Te treatment restored V_β and proliferation accompanied by parasympathetic innervation into the islets, and combination therapy was more effective against these measures in GK compared with GKTe. The ROC curve indicated that a cutoff value of 16.39 for IENFD was a good discrimination value for low V_β.

Diabetic insults pathologically injure peripheral nerves via mechanisms activated by hyperglycemia [29]. The vagal neural circuit is also disrupted by metabolic and immunologic disturbances caused by diabetes [20, 21]. In a previous study, the number of intracardiac neurons in GK were decreased compared with W at 9 months of age [30]. In our study, GK showed a marked loss of small PN fibers into the islets accompanied by a reduction of IENFD, correlating with V_β. In general, the loss of unmyelinated small fibers is an initial pathological change of DPN, which can be ameliorated by the early and intensified correction of hyperglycemia [31]. Ca ameliorated IENFD and PN density in GK despite no expression of SGLT2 in the nervous system [32]. This can be ascribed to a robust depletion of hyperglycemia exerted by Ca.

In contrast to SGLT2, GLP-1 receptors were identified on both peripheral and central nerves [33, 34]. Previous reports suggested that incretin-related compounds had direct neuroprotective effects independent of the blood glucose regulation in DPN models [28]. Interestingly, the highest secretion of active GLP-1 was observed in GKCaTe. Takebayashi et al. showed that administration of Ca before meal increased serum active GLP-1 level in Japanese T2DM patients [35]. Therefore, combination therapy of Ca and Te may have a strong impact for the regeneration and preservation of small fibers in T2DM via significant ameliorations of glycemic insults and an increase in active GLP-1 level.

Although Mundinger et al. showed no apparent sympathetic nerve reduction in the islets of T2DM autopsy cases [20], no data are collected regarding the density of PN in the islets of autopsy cases. GK shows a severe inflammatory reaction, fibrosis, and remodeling of the islet structure during T2DM progression [23, 26, 36], but these changes are not observed in human

specimens. Therefore, the reduction of parasympathetic innervation might be exaggerated in GK compared with humans. A brisk reduction of parasympathetic innervation may be observed, even in the human islets containing amyloid deposits, which usually show severe structural alterations. Recent evaluation applying transparent 3D histology elucidated rich parasympathetic innervation into the human islets, as observed in rodents [20]. The application of these new technologies may enable the evaluation of parasympathetic structural alterations in the islet caused by T2DM.

GLP-1 is a humoral factor that potentiates insulin secretion and β-cell protection in response to meal ingestion. It induces these effects via vagal nerve mediation as neuropeptides in the enter-insular axis [37]. Because these effects are mediated by the secretion of pituitary adenylate cyclase-activating polypeptide and vasoactive intestinal polypeptide from the nerve ends of activated efferent PNs [18], it is crucial that sufficient small PN fibers are arranged surrounding the islets to obtain enough stimulation of the β-cells in incretin therapy. The GLP-1 receptor is also expressed in β-cells, and its signaling deteriorates in hyperglycemic states. In combination therapy, SGLT2i effectively removes glucotoxicity by excreting glucose from the kidney, resulting in a possible increase in sensitivity of GLP-1 signaling in β-cells in the diabetic state.

SGLT2i administration could increase food intake despite decreased body weight in humans and rodents [38, 39]. A reduction in body weight and hyperphagia were also evident in GK treated with the therapy including Ca. Meanwhile, the mechanism is assumed to be insufficient calories due to excessive glucose excretion by Ca, the detailed mechanism has not been fully elucidated. Although there is a possibility that a dramatic metabolic shift to lipolysis and gluconeogenesis elicited by SGLT2i may decrease serum leptin, resulting in the induction of hyperphagia [40], a detailed analysis of the metabolic and hormonal changes in Ca-treated GK is necessary for future studies.

The effects of Ca were limited on V_{β} in GK despite the amelioration of glycemic control. In contrast, a previous study has shown the beneficial effects of SGLT2i on V_{β} in obese

experimental animals of T2DM [41]. This difference may be ascribed to the susceptibility of β-cell proliferation to intrinsic or extrinsic stimuli. In the obese model, the islets show brisk hyperplasia to adapt to severe insulin resistance in the peripheral tissue, whereas no adaptation is observed in GK [23,26,27]. Furthermore, V_{β} in GK was not restored by the simple amelioration of insulin resistance [36]. Therefore, the poor adaptive capability of β-cells in GK can contribute to the non-expansion of V_{β} in response to metabolic improvement obtained by Ca treatment. The other possibility is that a different metabolic state is evoked by SGLT2i between the obese and nonobese T2DM models. Obese diabetic model is generally prone to severe insulin resistance, hyperinsulinemia and continuous severe high blood glucose with dyslipidemia, whereas GK shows mild insulin resistance, low insulin secretion in response to glucose and moderate hyperglycemia. SGLT2i could improve those defects in obese T2DM because of significant promotion of fatty acid oxidation [42]. The peripheral, hypothalamic, and brainstem nutrient-sensing neurons form an interconnected network that monitors nutrient metabolism at different locations. The integration of these signals is finally converted into the activation or inhibition of the autonomic nervous. This system may not have functioned in GK as much as obese model because of different metabolic shift elicited by SGLT2i. Consequently, V_{β} might fail to be recovered despite the amelioration of parasympathetic innervation into the islets of GK treated with Ca.

It is known that several clinical parameters associating with glucose metabolism correlate with V_{β} in T2DM [4-6, 43]. Our results clearly showed that IENFD was a good discrimination factor of low V_{β} in GK. A cutoff value of 16.39 had high specificity and sensitivity for V_{β} discrimination. However, it remains unknown whether IENFD can be applied as a surrogate marker of V_{β} discrimination in human subjects. The diabetic pathophysiology of humans shows heterogeneity, while that of animal models is relatively uniform. Therefore, human IENFD shows a wide range, even in subjects with DPN in the same clinical stage [44]. GK is a

nonobese rodent T2DM model with insufficient insulin secretion in response to glucose [22]. These characteristics are similar to those of Japanese T2DM patients, showing a relatively low body mass index compared with Caucasians and insufficient insulin secretion in response to glucose [22,23,45]. Therefore, we regard GK as a reasonable model for Japanese T2DM. If restricted in the early stage of DPN in the Japanese population, which is expected not to be affected by various complicated metabolic disturbances, IENFD may be able to predict the cases of low V_{β}. Further study is required to confirm the utility of IENFD as a surrogate marker for low V_{β} in human T2DM.

This study has certain limitations that require consideration. First, there was no functional assessment of autonomic neuropathy in GK. Although we evaluated the pathological changes of the parasympathetic innervation of the islets, it is still unclear whether these changes may reflect other functional autonomic neuropathies. Second, in this protocol, we assessed the protective effects of Ca and Te rather than the therapeutic effects for T2DM treatment. In clinical settings, it is impractical to administer medication in the pre-diabetic state. Therefore, the effects of these compounds will need to be evaluated on established models of T2DM.

Overall, our results have clarified that the combination therapy of DPP4i and SGLT2i improved V_{β}, accompanied by PN density and IENFD. IENFD was proportionally correlated with V_{β}. Prevention of DPN development may be concurrently beneficial for the preservation of V_{β} in nonobese T2DM, whereas the value of IENFD may be a good surrogate marker to predict remaining V_{β} in nonobese T2DM.

Reference

1. Sakuraba H, Mizukami H, Yagihashi N, et al. Reduced beta-cell mass and expression of oxidative stress-related DNA damage in the islet of Japanese type II diabetic patients. Diabetologia. 2002; 45: 85-96
2. ButlerAE, JansonJ, Bonner-WeirS, et al. Beta-cell deficit and increased beta-cell apoptosis in humans with type 2 diabetes. Diabetes., 2003; 52: 102–110.
3. HenquinJC, RahierJ. Pancreatic alpha cell mass in European subjects with type 2 diabetes. Diabetologia., 2011; 54: 1720–1725.
4. Mizukami H, Takahashi K, Inaba W, et al. Involvement of oxidative stress-induced DNA damage, endoplasmic reticulum stress, and autophagy deficits in the decline of β-cell mass in Japanese type 2 diabetic patients. Diabetes Care., 2014; 37: 1966–1974.
5. Jurgens CA, Toukatly MN, Fligner CL, et al. β-cell loss and β-cell apoptosis in human type 2 diabetes are related to islet amyloid deposition. Am J Pathol., 2011; 178: 2632-2640.
6. Kamata K, Mizukami H, Inaba W, et al. Islet amyloid with macrophage migration correlates with augmented β-cell deficits in type 2 diabetic patients. Amyloid. 2014; 21: 191-201.
7. Xin A, Mizukami H, Inaba W, et al. Pancreas Atrophy and Islet Amyloid Deposition in Patients With Elderly-Onset Type 2 Diabetes. J Clin Endocrinol Metab., 2017; 102: 3162-3171.
8. Ahrén B. Autonomic regulation of islet hormone secretion – Implications for health and disease. Diabetologia, 2000; 43: 393-410.
9. Gilon P, Henquin J-C. Mechanisms and physiological significance of the cholinergic control of pancreatic beta-cell function. Endocr Rev, 2001; 22: 565-604.
10. Lindsay TH, Halvorson KG, Peters CM, et al. A quantitative analysis of the sensory and sympathetic innervation of the mouse pancreas. Neuroscience., 2006; 137: 1417-1426

11. Rodriguez-Diaz R, Caicedo A. Novel approaches to studying the role of innervation in the biology of pancreatic islets. Endocrinol Metab Clin North Am., 2013; 42: 39-56.
12. Thorens B. Neural regulation of pancreatic islet cell mass and function. Diabetes Obes Metab., 2014; Suppl 1: 87-95.
13. Kaneto A, Kosaka K, Nakao K. Effects of stimulation of the vagus nerve on insulin secretion. Endocrinology., 1967; 80: 530-536.
14. Niijima A. Nervous regulation of metabolism. Prog Neurobiol., 1989; 33: 135-147.
15. Kiba T, Tanaka K, Numata K, et al. Ventromedial hypothalamic lesion-induced vagal hyperactivity stimulates rat pancreatic cell proliferation. Gastroenterology., 1996; 110: 885-893.
16. Lausier J, Diaz WC, Roskens V, et al. Vagal control of pancreatic ß-cell proliferation. Am J Physiol Endocrinol Metab.,2010; 299: E786-793.
17. Imai J, Katagiri H, Yamada T, et al. Regulation of pancreatic beta cell mass by neuronal signals from the liver., Science, 2008; 322: 1250-1254.
18. Yamamoto J, Imai J, Izumi T, et al. Neuronal signals regulate obesity induced β-cell proliferation by FoxM1 dependent mechanism. Nat Commun. 2017; 8: 1930.
19. Tesfaye S, Boulton AJ, Dyck PJ, et al. "Diabetic neuropathies: update on definitions, diagnostic criteria, estimation of severity, and treatments,". Diabetes Care., 2010; 33: 2285-2293.
20. Mundinger TO, Mei Q, Foulis AK, et al. Human. Type 1 Diabetes Is Characterized by an Early, Marked, Sustained, and Islet-Selective Loss of Sympathetic Nerves. Diabetes., 2016; 65: 2322-2330.
21. Kohnert KD, Axcrona UM, Hehmke B, et al. Islet neuronal abnormalities associated with impaired insulin secretion in type 2 diabetes in the Chinese hamster. Regul Pept., 1999; 82: 71-79.
22. Portha B, Serradas P, Bailbé D, et al. Beta-cell insensitivity to glucose in the GK rat, a

spontaneous nonobese model for type II diabetes. Diabetes., 1991; 40: 486-491.

23. Koyama M, Wada R, Sakuraba H, et al. Accelerated loss of islet beta cells in sucrose-fed Goto-Kakizaki rats, a genetic model of non-insulin-dependent diabetes mellitus. Am J Pathol. 1998; 153: 537-545.
24. Fukuda-Tsuru S, Anabuki J, Abe Y, et al. A novel, potent, and long-lasting dipeptidyl peptidase-4 inhibitor, teneligliptin, improves postprandial hyperglycemia and dyslipidemia after single and repeated administrations. Eur J Pharmacol., 2012; 696: 194-202.
25. Liang Y, Arakawa K, Ueta K, et al. Effect of canagliflozin on renal threshold for glucose, glycemia, and body weight in normal and diabetic animal models. PLoS One., 2012; 7: e30555.
26. Inaba W, Mizukami H, Kamata K, et al. Effects of long-term treatment with the dipeptidyl peptidase-4 inhibitor vildagliptin on islet endocrine cells in non-obese type 2 diabetic Goto-Kakizaki rats. Eur J Pharmacol., 2012; 691: 297-306.
27. Mizukami H, Wada R, Koyama M, et al. Augmented beta cell loss and mitochondrial abnormalities in sucrose-fed GK rats. Virchows Arch., 2008; 452: 383-392.
28. Tsuboi K, Mizukami H, Inaba W, et al. The dipeptidyl peptidase IV inhibitor vildagliptin suppresses development of neuropathy in diabetic rodents: effects on peripheral sensory nerve function, structure and molecular changes. J Neurochem., 2016; 136: 859-870.
29. Yagihashi S. Glucotoxic Mechanisms and Related Therapeutic Approaches. Int Rev Neurobiol., 2016; 127: 121-149.
30. Batulevicius D, Frese T, Peschke E, et al. Remodelling of the intracardiac ganglia in diabetic Goto-Kakizaki rats: an anatomical study. Cardiovasc Diabetol., 2013; 12: 85.
31. Azmi S, Ferdousi M, Petropoulos IN, et al. Corneal confocal microscopy shows an improvement in small-fiber neuropathy in subjects with type 1 diabetes on continuous subcutaneous insulin infusion compared with multiple daily injection. Diabetes Care., 2015; 38: e3-4.

32. Wright EM, Turk E. The sodium/glucose cotransport family SLC5. Pflügers Archiv., 2004; 447: 510-518.
33. Kumari P, Nakata M, Zhang BY, et al. GLP-1 receptor agonist liraglutide exerts central action to induce β-cell proliferation through medulla to vagal pathway in mice. Biochem Biophys Res Commun., 2018; 499: 618-625.
34. Charpentier J, Waget A, Klopp P, et al. Lixisenatide requires a functional gut-vagus nerve-brain axis to trigger insulin secretion in controls and type 2 diabetic mice. Am J Physiol Gastrointest Liver Physiol., 2018; 315: G671-G684.
35. Takebayashi K, Hara K, Terasawa T, et al. Effect of canagliflozin on circulating active GLP-1 levels in patients with type 2 diabetes: a randomized trial. Endocr J., 2017; 64: 923-931.
36. Mizukami H, Wada R, Yonezawa A, et al. Suppression of post-prandial hyperglycaemia by pioglitazone improved islet fibrosis and macrophage migration in the Goto-Kakizaki rat. Diabetes Obes Metab., 2008; 10: 791-794.
37. Nishizawa M, Nakabayashi H, Uehara K, et al. Intraportal GLP-1 stimulates insulin secretion predominantly through the hepatoportal-pancreatic vagal reflex pathways. Am J Physiol Endocrinol Metab., 2013; 305: E376-387.
38. Devenny JJ, Godonis HE, Harvey SJ, et al. Weight loss induced by chronic dapagliflozin treatment is attenuated by compensatory hyperphagia in diet-induced obese (DIO) rats. Obesity (Silver Spring), 2012; 20:1645–1652.
39. Komiya C, Tsuchiya K, Shiba K, et al. Ipragliflozin improves hepatic steatosis in obese mice and liver dysfunction in type 2 diabetic patients irrespective of body weight reduction. PLoS ONE 2016; 11(3): e0151511.
40. Garvey WT, Van Gaal L, Leiter LA, et al. Effects of canagliflozin versus glimepiride on adipokines and inflammatory biomarkers in type 2 diabetes. Metabolism, 2018; 85: 32-37.
41. Millar PJ, Pathak V, Moffett RC, et al. Beneficial metabolic actions of a stable GIP agonist following pre-treatment with a SGLT2 inhibitor in high fat fed diabetic mice. Mol Cell

Endocrinol., 2016; 420: 37-45.

42. Osataphan S, Macchi C, Singhal G, et al. SGLT2 inhibition reprograms systemic metabolism via FGF21-dependent and -independent mechanisms. JCI Insight., 2019; 4(5): 123130.
43. Fujita Y, Kozawa J, Iwahashi H, et al. Increment of serum C-peptide measured by glucagon test closely correlates with human relative beta-cell area. Endocr J., 2015; 62: 329-337.
44. McArthur JC, Stocks EA, Hauer P, et al. Epidermal nerve fiber density: normative reference range and diagnostic efficiency. Arch Neurol., 1998; 55(12): 1513-1520.
45. Møller JB, Pedersen M, Tanaka H, et al. Body composition is the main determinant for the difference in type 2 diabetes pathophysiology between Japanese and Caucasians. Diabetes Care.; 2014; 37: 796-804.

Figure legends

Figure 1. Effects of SGLT2i, DPP4i, and combination therapy on blood glucose concentrations and insulin secretion during a 2 g/kg OGTT

At the beginning of the experiment, GK exhibited significant hyperglycemia after the glucose challenge (**A**). After 24week treatment, Te and Ca significantly suppressed the increases in blood glucose concentrations after glucose challenge (**B**). Combination therapy the most improved the increase in blood glucose after glucose challenge among all groups (**B**). Fasting serum insulin (left) and serum insulin 15 min. after glucose challenge (right) were shown (**C**). Fasting serum insulin was comparable between W and GK. Fasting serum insulin was significantly suppressed in GKCa compared to GK ($p < 0.05$) (**C**). GKCaTe showed similar tendency to GKCa, but it was not significant. GK showed significantly lower serum insulin compared with W ($p < 0.01$) 15 min after 2g/kg glucose challenge. Insulin of Ca was similar to GK. Te significantly increased insulin compared to GK ($p < 0.05$). Combination therapy further potentiated insulin than Te ($p < 0.05$) (**C**). Δ15 min. insulin secretion (15 min. insulin value minus 0 min. insulin value) after the glucose challenge was significantly decreased in GK compared to W (**D**). Δ15 min. insulin secretion in GKCa was similar to that of GK, while, Te significantly increased Δ15 min. insulin secretion compared to GK ($p < 0.01$). Combination therapy the most potentiated Δ15 min. insulin secretion after glucose challenge (**D**). W, untreated Wistar rats; GK, Goto-Kakizaki rats; GKCa, canagliflozin-treated GK rats; GKTe, teneligliptin-treated GK rats; GKCa, both canagliflozin, and teneligliptin-treated GK rats. Data are presented as the mean ± SE. Analysis of variance with Tukey's test was performed; $^{*}p < 0.01$ vs. W, $^{\dagger}p < 0.05$ vs. GK, $^{\ddagger}p < 0.01$ vs. GK, $^{\S}p < 0.05$ vs. GKTe, $^{\#}p < 0.01$ vs. GKTe, $^{**}p < 0.01$ vs. GKCa, $^{\dagger\dagger}p < 0.05$ vs. GKCa.

Figure 2. Islet structure and endocrine cell composition in the experimental animals

H&E section from GK showing oval or round islets with a smooth contour at 5 weeks of age, similar to W (**A**). Five-color immunostaining showed β-cells (black) located in

the center of the islets and α- (red), δ- (green), and PP-cells (blue) at the periphery in both W and GK (**B**). Ki-67-positive β-cells (arrow, brown) were abundantly observed in both GK and W (**B**). The islets in GK became fibrotic with an irregular circumference at 29 weeks of age compared with W **(C)**. Ca improved fibrosis, but the islet cell volume was similar to GK, whereas Te and combination therapy increased islet cell volume (**C**). Disturbed islet endocrine cell polarization was ameliorated in Ca and Te monotherapy and combination therapy for both (**D**). W, untreated Wistar rats; GK, Goto-Kakizaki rats; GKCa, canagliflozin-treated GK rats; GKTe, teneligliptin-treated GK rats; GKCaTe, both canagliflozin- and teneligliptin-treated GK rats. Scale bar represents 50 μm.

Figure 3. β-cell proliferation in experimental animals of 29 weeks of age

Five-color immunohistochemistry revealed Ki67-positive endocrine cells in the islets (**A**). Proliferative β-cells stained brown for Ki67 and black for insulin (yellow arrow) and were easily detected in W. The frequency of Ki67-positive β-cells was sparse in GK and GKCa. Te and combination treatment improved β cell proliferation in GK. W, untreated Wistar rats; GK, Goto-Kakizaki rats; GKCa, canagliflozin-treated GK rats; GKTe, teneligliptin-treated GK rats; GKCaTe, both canagliflozin- and teneligliptin-treated GK rats. Scale bar represents 50 μm.

Figure 4. Representative immunohistochemical sections of PN innervation into the islet labeled by VAChT antibody in experimental animals

VAChT-positive PN fibers were observed as red dots (arrows and inset) in the islets (**A to G**). PN fibers were labeled with VAChT antibody in the islets of both W (**A**) and GK (**B**) at the beginning of the experiment (0 weeks). The densities of PN fibers were similar between two groups (**H**). At the end of the experiment (24 weeks), density of parasympathetic innervation was significantly decreased in GK (**D**) compared to W (**C and I**). Ca (**E**) and Te

(**F**) could significantly increase the density and combination therapy (**G**) improved the density similar to that of W (**I**). V_{β} was proportionally correlated with the density of PN ($R = 0.55$, $p < 0.01$) (**J**). W, untreated Wistar rats; GK, Goto-Kakizaki rats; GKCa, canagliflozin-treated GK rats; GKTe, teneligliptin-treated GK rats; GKCaTe, both canaglifolozin- and teneligliptin-treated GK rats. Values are means ± SE. Analysis of variance with Tukey's test for multiple comparisons, and association between PN density and V_{β} was estimated by liner regression analysis using StatView 5.0.1 software ; $^{*}p < 0.01$ vs. W, $^{\dagger}p < 0.05$ vs. GK, $^{\ddagger}p < 0.01$ vs. GK, $^{\S}p < 0.05$ vs. GKCa and GKTe. Scale bar represents 50 μm.

Figure 5. Functional and pathological evaluation of peripheral nerves in experimental animals of 5 weeks of age

The MNCV and SNCV of GK were comparable with those of W at 5 weeks of age (**A and B**). Thermal latency was evaluated by the tail-flick test and was comparable between W and GK (**C**). IENFD was evaluated with double immunofluorescence for the unmyelinated small fibers labeled with anti-PGP9.5 (arrow, red) and the epidermis with anti-CK 5/6 (green) (**D**). IENFD was also similar between W and GK (**D and E**). Values are presented as mean ± SE. W, untreated Wistar rats; GK, Goto-Kakizaki rats. Scale bar represents 50 μm.

Figure 6. Evaluation of peripheral nerve function and pathology

MNCV and SNCV were comparable among all groups at 24 weeks of the experiments (**A**). The tail-flick test revealed thermal perception threshold in GK increased 2.5times than W ($p < 0.01$) (**B**). This increase was gradually improved by monotherapy of Ca and Te, and combination therapy. Intraepidermal nerve fiber was visualized by double immunofluorescence to the nerve fiber (arrow, red) and epidermis (green) (**C**). IENFD was reduced in GK compared to W ($p < 0.01$) (**C and D**). Monotherapy similarly improved the

reduction ($p < 0.05$ vs. GK, respectively, **D**). Combination therapy had the greatest effects on IENFD of GK ($p < 0.01$ vs. GKCa and $p < 0.05$ vs. GKTe, **D**). IENFD proportionally correlated with V_{β} ($r = 0.54$, $p < 0.01$) (**E**). ROC curve between V_{β} and IENFD showed the AUC was 0.87, when low V_{β} was defined as less than 1.28 (**F**). The sensitivity and specificity of the test at cutoff value of 16.39 were 0.86 and 0.82 respectively. Values are mean ± SE. Analysis of variance with Tukey's test for multiple comparisons and liner regression test for **E** and ROC curve analysis for **F** were performed using JMP 10.0.4 software; W, untreated Wistar rats; GK, Goto-Kakizaki rats; GKCa, canagliflozin-treated GK rats; GKTe, teneligliptin-treated GK rats; GKCa, both canagliflozin- and teneligliptin- treated GK rats. $^{*}p < 0.01$ vs. W, $^{\dagger}p < 0.05$ vs. GK, $^{\ddagger}p < 0.01$ vs. GKCa and GKTe, $^{\S}p < 0.01$ vs. GKCa and $p < 0.05$ vs GKTe. Scale bar represents 50 μm.

Figure 1

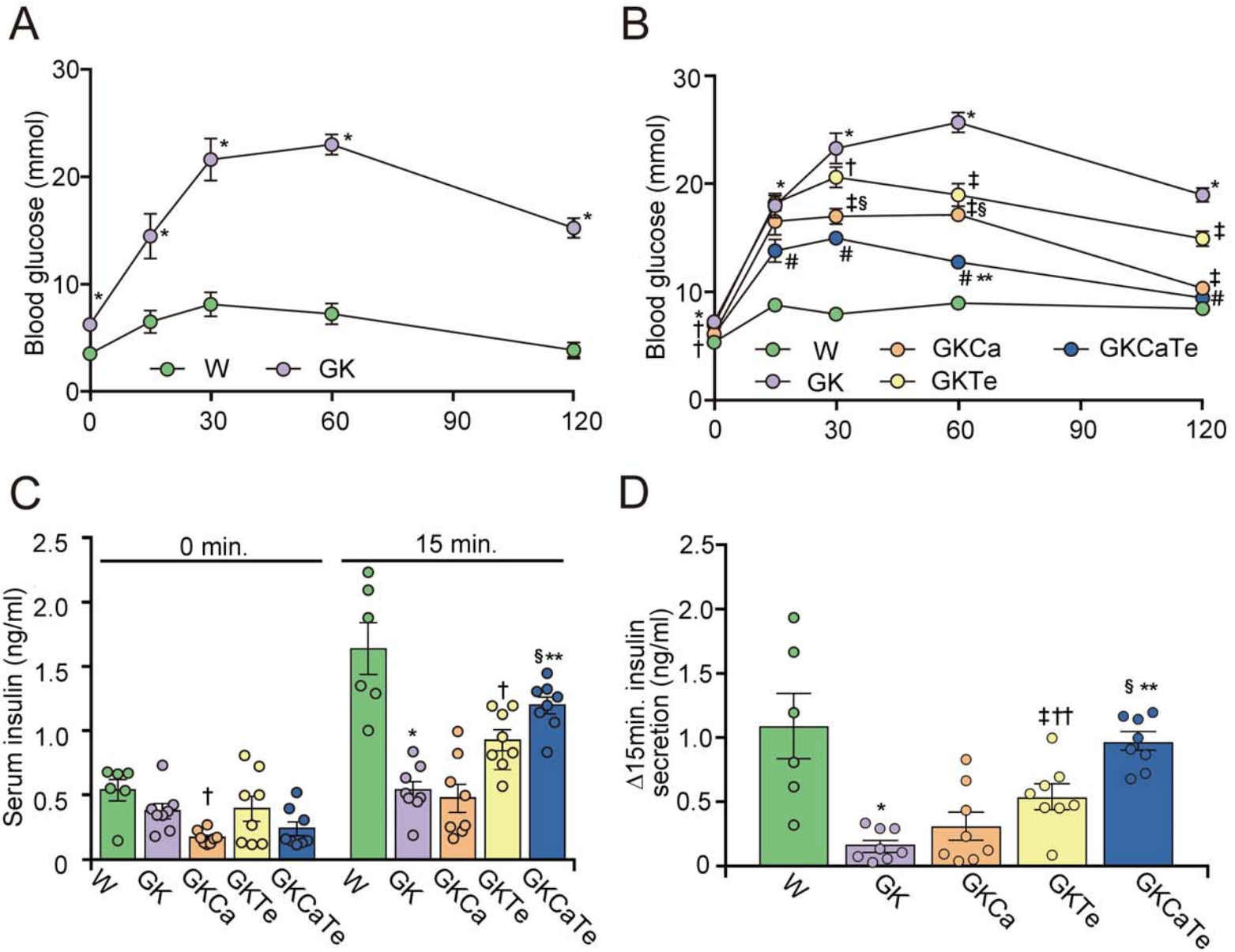
A
Blood glucose (mmol)
W
GK
B
GKCa
GKCaTe
GKTe
C
0 min.
15 min.
Serum insulin (ng/ml)
W
Gk
GKCa
GKTe
GKCaTe
D
Δ15min. insulin secretion (ng/ml)

Figure 2.

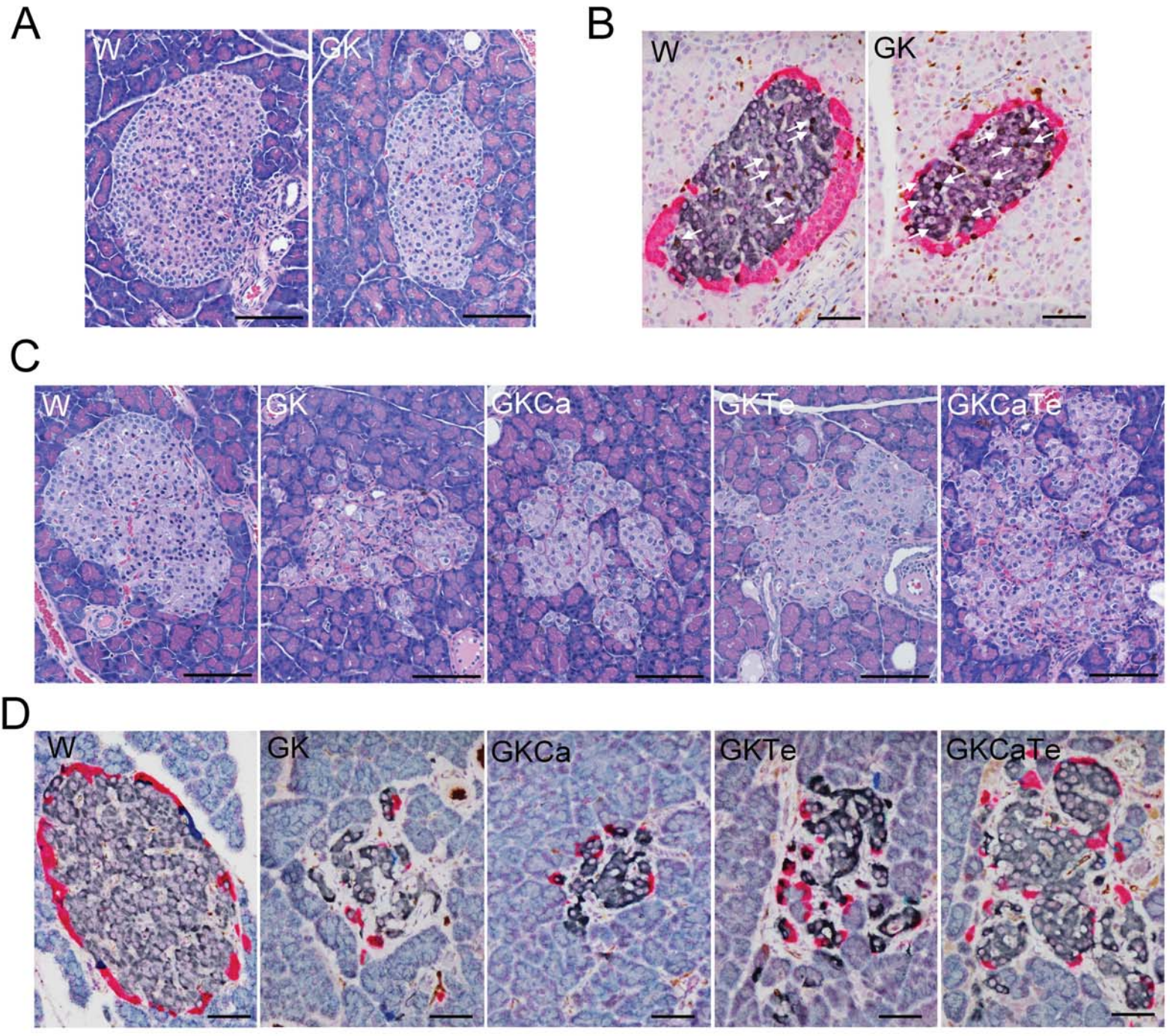

Figure 3.

A

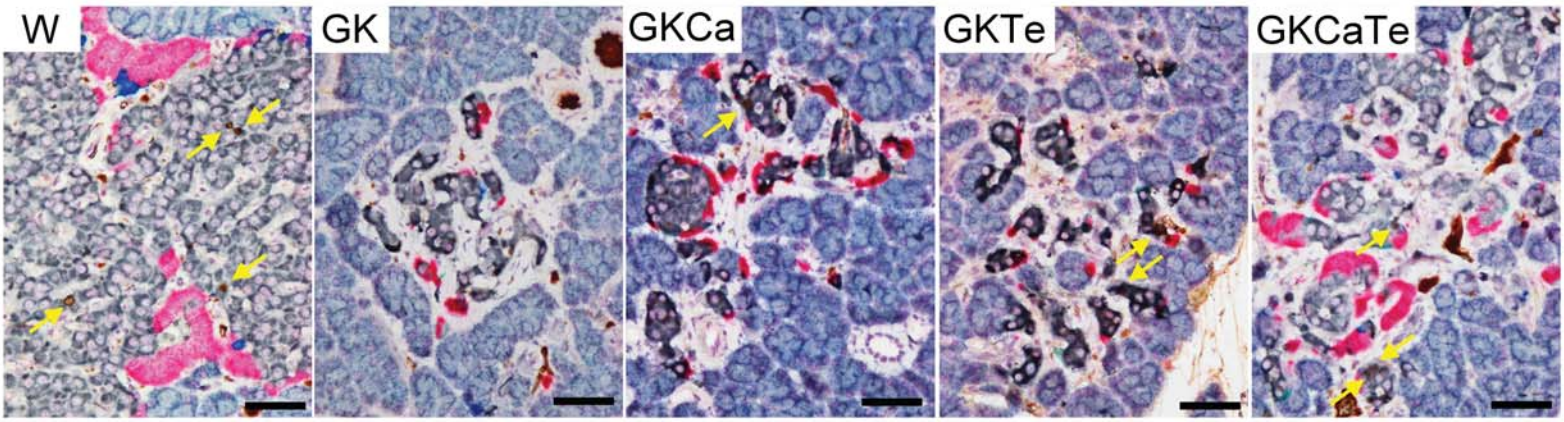

Figure 4

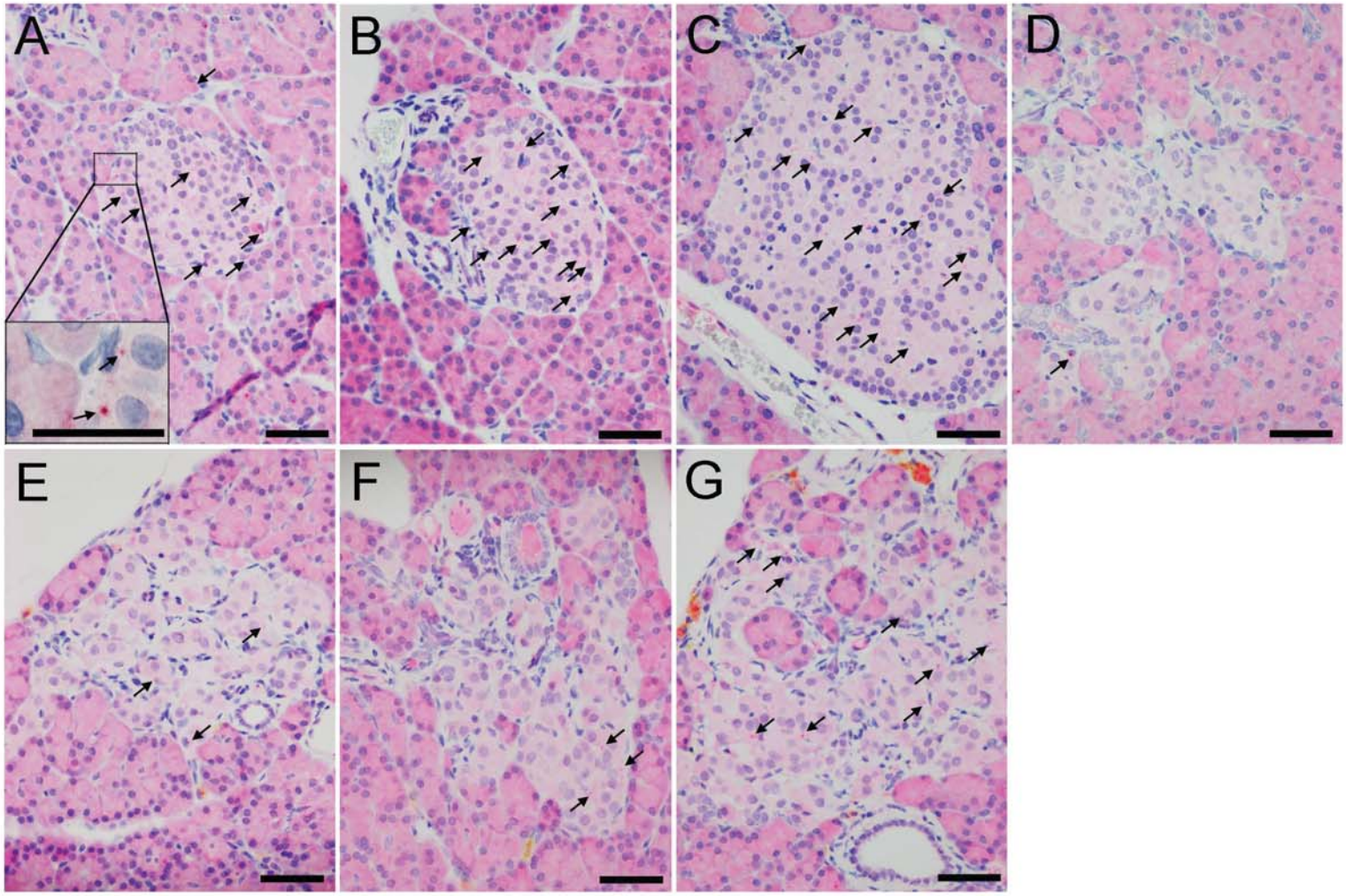
A
B
C
D
E
F
G

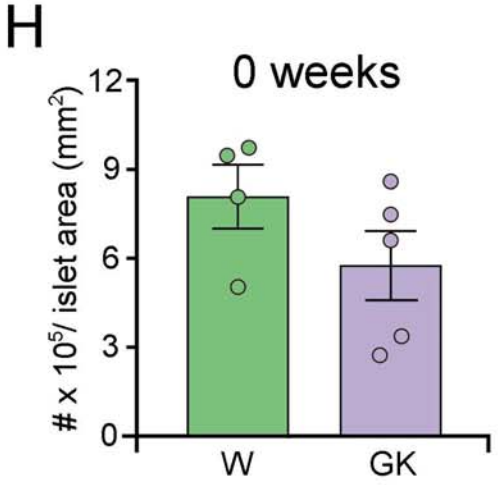
H
0 weeks
x 10^5/ islet area (mm^2)
12
9
6
3
0
W
GK

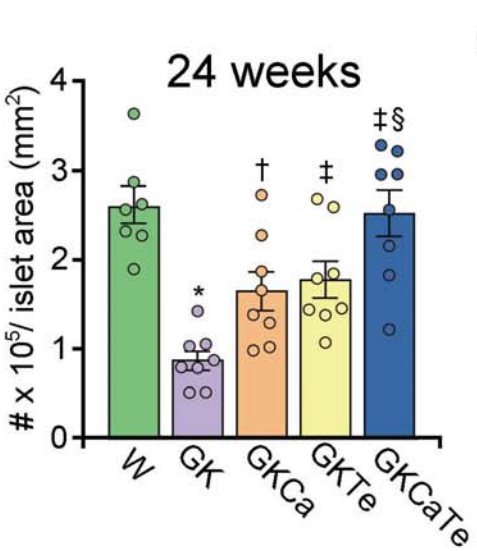
I
24 weeks
x 10^5/ islet area (mm^2)
4
3
2
1
0
*
†
‡
‡§
W
GK
GKCa
GKTe
GKCaTe

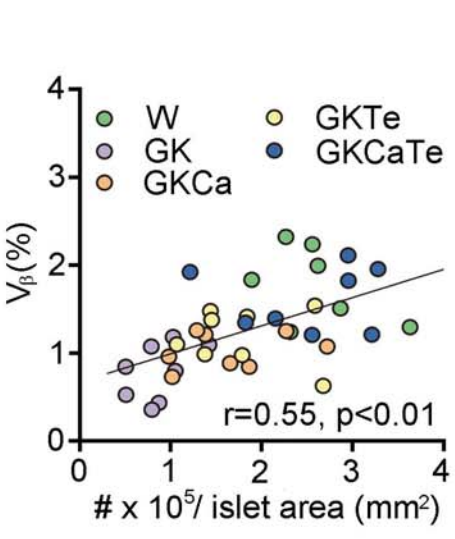
J
W
GK
GKCa
GKTe
GKCaTe
Vβ(%)
r=0.55, p<0.01
0
1
2
3
4
x 10^5/ islet area (mm^2)

Figure 5.

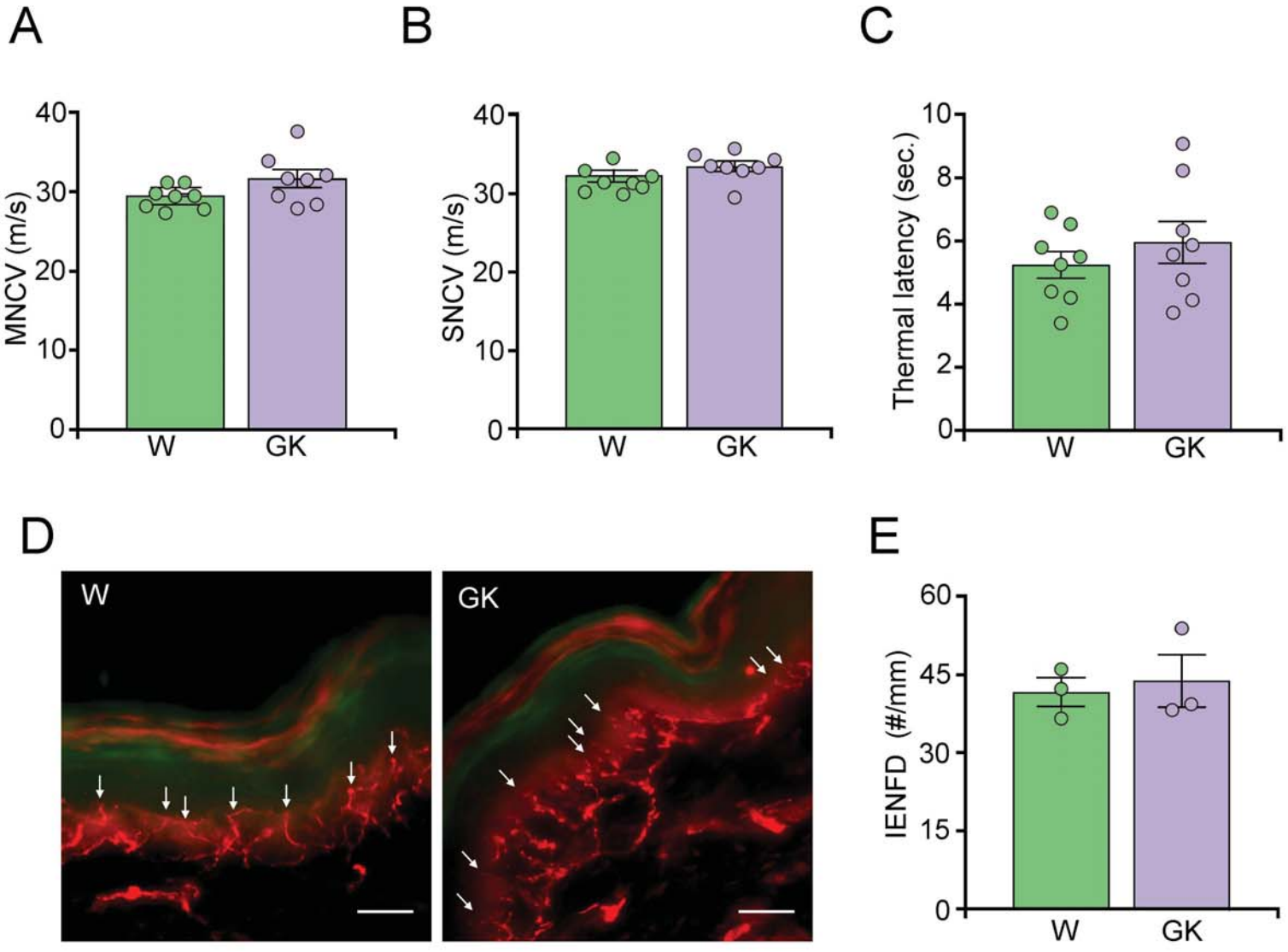
A
MNCV (m/s)
40
30
20
10
0
W
GK
B
SNCV (m/s)
40
30
20
10
0
W
GK
C
Thermal latency (sec.)
10
8
6
4
2
0
W
GK
D
W
GK
E
IENFD (#/mm)
60
45
30
15
0
W
GK

Figure 6

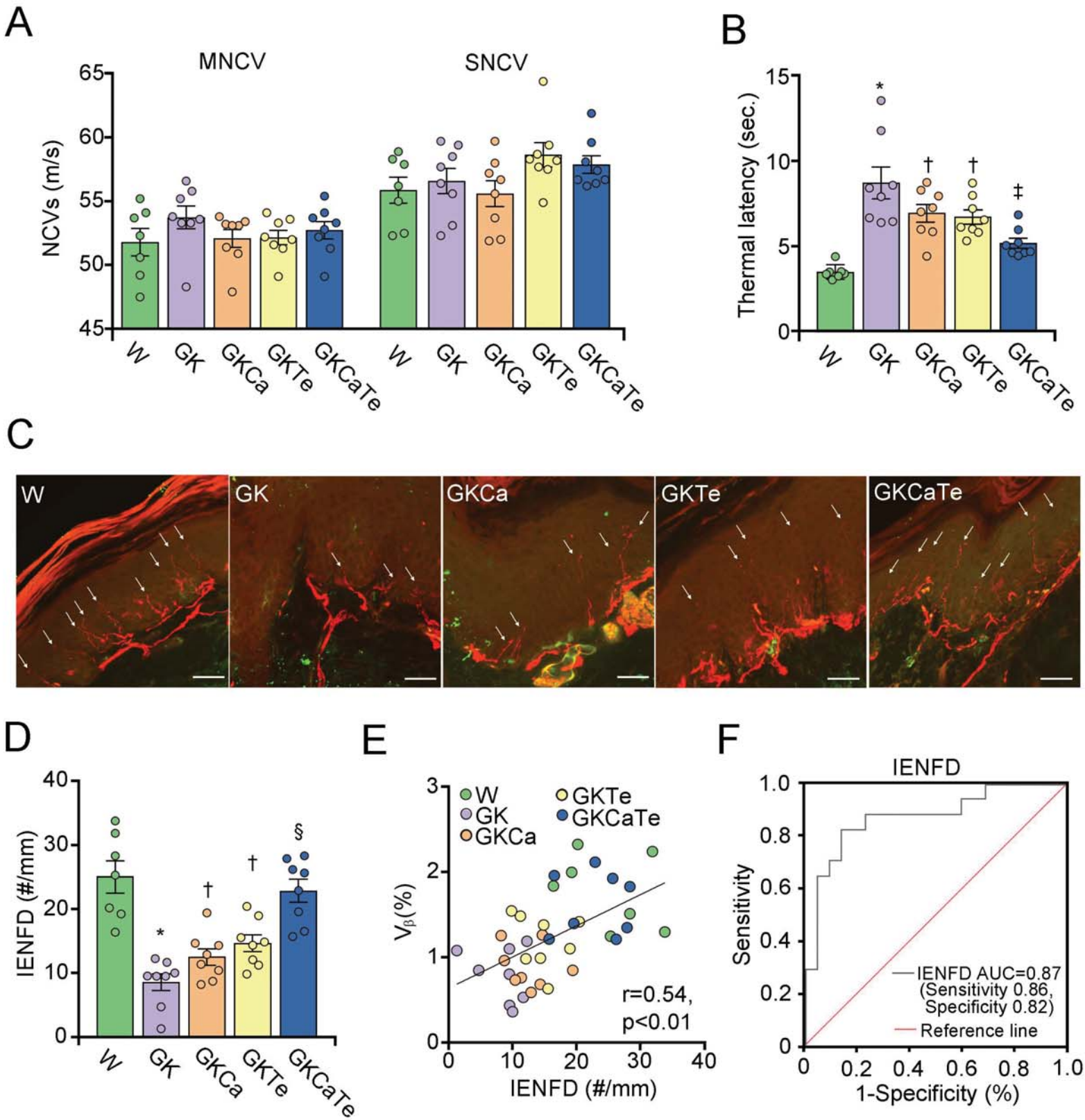
A
MNCV
SNCV
NCVs (m/s)
65
60
55
50
45
W
GK
GKCa
GKTe
GKCaTe
B
Thermal latency (sec.)
15
10
5
0
*
†
‡
C
W
GK
GKCa
GKTe
GKCaTe
D
IENFD (#/mm)
40
30
20
10
0
*
†
§
E
W
GK
GKCa
GKTe
GKCaTe
Vβ(%)
r=0.54,
p<0.01
IENFD (#/mm)
F
IENFD
Sensitivity
1-Specificity (%)
IENFD AUC=0.87
(Sensitivity 0.86,
Specificity 0.82)
Reference line

Table 1. Antibody list

Antibody name	Species	Catalog No.	Vendor	Experiments	Dilutions
insulin	Rabbit	ab181547	Abcam (Cambridge, United Kingdom)	IHC	1:4000
glucagon	Rabbit	ab92517	Abcam (Cambridge, United Kingdom)	IHC	1:15000
somatostain	Mouse	sc-55565	Santa Cruz biotechnology, Inc. (CA, USA)	IHC	1:250
pancreatic polypeptide (PP)	Rabbit	#16081	Immuno-Biological Laboratories Co., Ltd. (Gunma, Japan)	IHC	1:3000
Ki-67	Rabbit	ab15580	Abcam (Cambridge, United Kingdom)	IHC	1:250
vesicular acetylcholine transporter (VachT)	Goat	abn100	Merck KGaA, (Darmstadt, Germany)	IHC	1:500
protein gene product 9.5 (PGP 9.5)	Rabbit	Z5116	Agilent (CA, USA)	IF	1:1000
cytokeratin 5/6 (CK 5/6)	Mouse	MAB1910	Agilent (CA, USA)	IF	1:1000

IHC; immunohistochemistry, IF; immunofluorescence.

Table 2. Clinical parameters for experiment animals

	W	GK	GKCa	GKTe	GKCaTe
Body weight (g)					
Start (0 weeks)	97.4±11.7 (n=8)	92.96±7.9 (n=8)			
End (24 weeks)	458.8±31.8 (n=7)	390.1±19.0* (n=8)	364.5±14.8†(n=8)	378.5±12.5 (n=8)	358.6±16.3‡§ (n=8)
Food intake (g/day)					
Start (0 weeks)	5.5±0.6 (n=8)	6.1±0.1 (n=8)			
End (24 weeks)	5.9±0.5 (n=7)	6.2±0.9 (n=8)	10.1±0.5† (n=8)	6.8±0.8 (n=8)	9.8±0.9†§ (n=8)
Fasting blood glucose (mmol/L)					
Start (0 weeks)	3.6±0.1 (n=8)	6.3±0.6* (n=8)			
End (24 weeks)	5.4±0.2 (n=7)	7.3±0.3* (n=8)	6.2±0.5† (n=8)	8.0±0.3 (n=8)	6.1±0.4$^{\dagger\#}$ (n=8)
Fed blood glucose (mmol/L)					
Start (0 weeks)	6.1±0.2 (n=8)	8.6±0.4* (n=8)			
End (24 weeks)	8.5±0.2 (n=7)	14.3±0.2* (n=8)	10.5±0.6‡ (n=8)	12.8±0.4† (n=8)	10.6±0.5$^{\ddagger\#}$ (n=8)
HbA1c (%) (24 weeks)	3.3±0.1 (n=7)	4.5±0.1* (n=8)	3.9±0.1‡ (n=8)	4.2±0.1† (n=8)	3.7±0.1$^{\ddagger\#}$ (n=8)
Active GLP-1 (pg/mL) (24 weeks)					
Fasting	1.0±0.2 (n=7)	1.1±0.2 (n=8)	0.7±0.1 (n=8)	7.7±1.2‡ (n=8)	9.7±0.9‡§,** (n=8)
2g/kg Glucose stimulation	2.0±0.5 (n=7)	2.4±0.4 (n=8)	1.8±0.3 (n=8)	11.1±2.2† (n=8)	21.1±2.0‡§,** (n=8)

Values are expressed as means ± S.E. W, untreated Wistar rats; GK, Goto-Kakizaki rats; GKCa, canagliflozin-treated GK rats; GKTe, teneligliptin-treated GK rats; GKCaTe, both canagliflozin and teneligliptin-treated GK rats. Analysis of variance with Tukey's test for multiple comparisons. *p<0.01 vs W, †p<0.05 vs GK, ‡p<0.01 vs GK, §p<0.05 vs GKTe, $^{\#}$p<0.01 vs GKTe, **p<0.01 vs GKCa.

Table 3. Morphometric analysis of islets in experiment animals

Cell volume density (5 weeks of age)					
Group	**W (n=8)**	**GK (n=8)**	**GKCa**	**GKTe**	**GKCaTe**
V_β (%)	0.75±0.12	0.72±0.02	N.A.	N.A.	N.A.
V_α (%)	0.46±0.05	0.40±0.03	N.A.	N.A.	N.A.
V_δ (%)	0.03±0.01	0.03±0.01	N.A.	N.A.	N.A.
V_{pp} (%)	0.01±0.01	0.01±0.01	N.A.	N.A.	N.A.
Cell volume density (29 weeks of age)					
Group	**W (n=7)**	**GK (n=8)**	**GKCa (n=8)**	**GKTe (n=8)**	**GKCaTe (n=8)**
V_β (%)	1.78±0.17	0.82±0.11*	1.03±0.07	1.19±0.11†	1.62±0.13$^{\ddagger\S\#}$
V_α (%)	0.68±0.07	0.43±0.06*	0.49±0.05	0.53±0.07	0.62±0.04†§
V_δ (%)	0.08±0.01	0.07±0.01	0.05±0.01	0.08±0.02	0.09±0.01
V_{pp} (%)	0.08±0.01	0.01±0.01*	0.01±0.01*	0.01±0.01*	0.01±0.01*
Insulin contents (ng/pancreas)	377.56±24.20	168.48±20.90*	194.28±17.82	246.87±22.59†	322.01±26.04$^{\ddagger\S\#}$
Ki67 index (5 weeks of age)					
Group	**W (n=8)**	**GK (n=8)**	**GKCa**	**GKTe**	**GKCaTe**
β cell (%)	6.90±0.82	7.08±0.37	N.A.	N.A.	N.A.
α cell (%)	7.32±0.54	9.67±0.30*	N.A.	N.A.	N.A.
δ cell (%)	0	0	N.A.	N.A.	N.A.
pp cell (%)	0	0	N.A.	N.A.	N.A.
Ki67 index (29 weeks of age)					
Group	**W (n=7)**	**GK (n=8)**	**GKCa (n=8)**	**GKTe (n=8)**	**GKCaTe (n=8)**
β cell (%)	0.27±0.03	0.08±0.02*	0.09±0.03*	0.18±0.03†	0.27±0.03$^{\ddagger\S\#}$
α cell (%)	0.37±0.05	0	0	0	0.04±0.02
δ cell (%)	0.22±0.09	0	0	0.06±0.06	0.12±0.12
pp cell (%)	0.28±0.14	0	0	0	0

Values are expressed as means±S.E. W, untreated Wistar rats; GK, Goto-Kakizaki rats; GKCa, canagliflozin-treated GK rats; GKTe, teneligliptin-treated GK rats; GKCaTe, both canagliflozin and teneligliptin-treated GK rats; N.A., not applicable. Analysis of variance with Tukey's test for multiple comparisons. $^{*}p<0.01$ vs W, $^{\dagger}p<0.05$ vs GK, $^{\ddagger}p<0.01$ vs GK, $^{\S}p<0.05$ vs Ca, $^{\#}p<0.05$ vs Te.